Journal of
Biomedical Nanotechnology
Vol. 3, 1–4, 2007

Multi-Walled Carbon Nanotubes Interact with Cultured Rice Cells: Evidence of a Self-Defense Response

Xiao-ming Tan and Bunshi Fugetsu*

Laboratory of Environmental Medical Chemistry, Graduate School of Environmental Science, Hokkaido University, Sapporo 060-0810, Japan

Multi-walled carbon nanotubes (MWCNTs) are widely used in nanotechnology despite concerns about possible toxic effects. To determine whether MWCNTs are toxic to rice, rice cells (*Oryza sativa L.*) were cultured with MWCNTs. Rice cells interacted with MWCNTs to form aggregates that were observed using light and scanning electron microscopy. Cell density decreased with increased MWCNT concentration, possibly indicating a self-defense response. Thus, MWCNTs interact directly with rice cells and may have a detrimental effect on rice growth. This effect, although, was stronger than that found for carbon blacks, the rice cells survived the MWCNTs through the self-defense response.

Keywords: Multi-Walled Carbon Nanotubes (MWCNTs), Rice (*Oryza sativa L.*) Cells, Non-Specific Interaction, Self-Defense Response.

1. INTRODUCTION

Developments in nanotechnology have led to predictions of great benefits as well as to warnings of great dangers to humanity and the environment. Carbon nanotubes (CNTs) have novel properties that are keys for many nanotechnology applications, and it is thought that tens or even hundreds of tons of CNTs will be produced worldwide within a few years.[1] This increase in CNT production will undoubtedly increase the exposure of humans and the environment to CNTs. A recent study found that the natural organic matter present in river water was capable of both stabilizing and dispersing CNTs.[2] Thus, if CNTs are toxic, their influence in the environment will be long lasting and could spread throughout the food chain. In fact, several studies on nanotoxicity have suggested that CNTs can adversely affect both humans and animals.[3–9] Bottini and co-workers evaluated the toxicity of pristine and oxidized multi-walled CNTs (MWCNTs) on human T cells.[3] They found that the latter are toxic and can induce massive loss of cell viability through programmed cell death at doses of 400 μg/ml, corresponding to approximately 10 million CNTs per cell. Muller et al. reported that Sprague–Dawley rats develop inflammation and fibrotic reactions after 60 days of exposure to CNTs.[5] Toxicity studies have thus far focused on the responses of organisms and/or specialized animal and human cells to CNT exposure.

In this study, we investigated whether MWCNTs are toxic to plants, using one of the most important crops in the world, rice, as a representative example. Hundreds of tons of MWCNTs have been used worldwide, so their possible impact on agriculture is of great interest. Studies were carried out by culturing cell suspensions of rice in the presence of MWCNTs. Our results showed interactions between rice cell and MWCNTs and provided new insights into the rice self-defense system.

2. EXPERIMENTAL PROCEDURES

Mature rice embryos (*Oryza sativa L.*) were grown on Murashige and Skoog (MS) solid medium for callus induction.[10] After three months, established calli were separated from friable calli and transferred to AA liquid medium[11] for cell suspension culture. After ten days, MWCNTs were added to the AA liquid medium and dispersed by ultra-sonication. Three groups of five 10 ml samples were prepared: Group A had 0.05 g/l MWCNTs, Group B had 0.1 g/l MWCNTs, and Group C, the control, had no MWCNTs. These three groups of five samples were placed on a rotary shaker at 120 rpm in the dark. After 4 days of incubation, the samples were examined using light microscopy; cell density was also determined using an hemocytometer. For density determination, the cells in each sample were counted five times, and the greatest and smallest values ignored. Three values were thus used to determine the average density for each sample.

*Author to whom correspondence should be addressed.

RESEARCH ARTICLE

Table I. Dimensions and surface area of MWCNTs and carbon blacks used in this study.

Carbon materials	Dimensions	Surface area
MWCNT	20–40 nm × 0.50–50 μm	3.14×10^{-2}–6.28 μm^2
Carbon black	ϕ100–200 nm	0.031–0.126 μm^2

Comparison studies were conducted using carbon blacks (these partial-like materials have been the industrially utilized structural or conductive filler in plastics) as the reference samples. Table I summarizes the physical dimensions and the surface area. The surface area was calculated as either cylinders (MWCNTs) or spheres (carbon blacks). The possible reminded catalytic metals in the samples were removed by refluxing the carbon nano-materials in 4 M hydrochloric acid for approximately 20 hours.[12]

3. RESULTS AND DISCUSSION

The cell density in Groups A and B was much lower than in control Group C (Table II). Moreover, as the concentration of MWCNTs increased from 0.05 g/l to 0.1 g/l (two-fold), the cell density was reduced from 38 to 27 (71%). Light microscopy revealed many black clumps in the samples in Groups A and B, as well as cells that were not associated with MWCNTs (Fig. 1). Scanning electron microscopy (SEM) images confirmed that these black clumps were MWCNTs that were tightly wrapped around and associated with the cells (Fig. 2). The number and the size of the black clumps in sample B were much greater than in sample A, and the percentage of the area of the cells covered by MWCNTs ranged from 0 to 100%; in some instances, the covered area was greater than 100% due to multiple layers of MWCNTs (see Fig. 1). It also seemed that once cells were associated with MWCNTs, further association was more likely until finally an aggregate or precipitate formed. In other words, when MWCNTs were added to the culturing solution, all the cells in suspension would theoretically have an equal probability of making contacting with them. However, only part of the cell population interacted with MWCNTs, and the cells that first associated with MWCNTs were then more likely to form even more associations until they were covered completely. As the cells combined with MWCNTs, the size of the cell/MWCNT aggregates (i.e., the black clumps) became larger until the aggregates were precipitated from the cell culture.

Table II. The effects of MWCNTs on the density of cultured rice cells grown in suspension. Carbon blacks were used as the reference for comparison.

Density cells/1 μl	1	2	3	4	5	Average density
Group A[a]	45	41	36	38	29	38
Group B[b]	25	78	28	15	28	27
Group R1[c]	52	31	50	34	86	45
Group R2[d]	47	30	72	17	32	36
Group C[e]	69	31	93	65	130	76

[a]Group A: 0.05 g/L MWCNTs. [b]Group B: 0.10 g/L MWCNTs. [c]Group R1: 0.05 g/L carbon blacks. [d]Group R2: 0.1 g/L carbon blacks. [e]Control samples (Group C): no MWCNTs. For each sample (5 samples/group), five density measurements were done. The largest and smallest values were ignored, and the three remaining values were used to calculate the average value (columns 1–5). These average values were used to calculate the average cell density for the group (rightmost column).

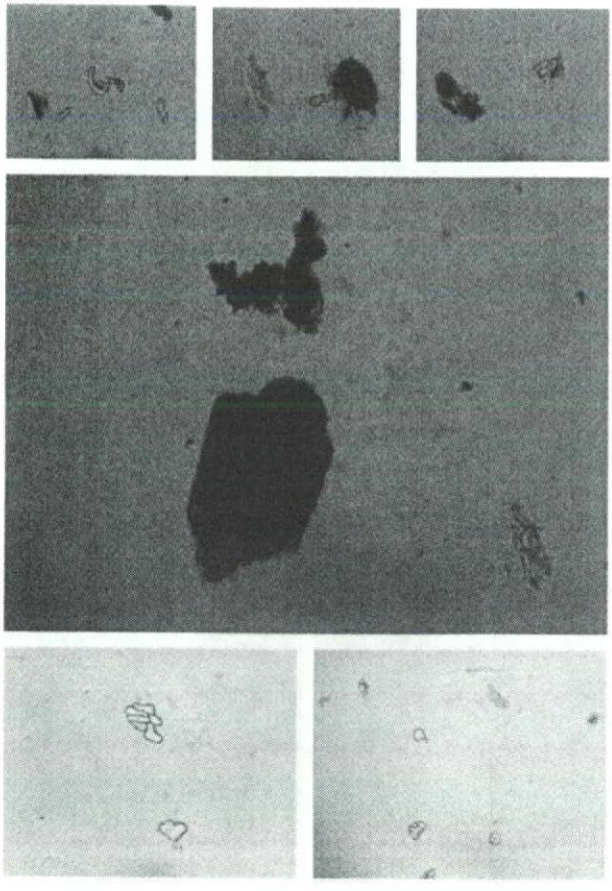

Fig. 1. Samples of cultured rice cells from Group A (0.05 g/L MWCNTs), B (0.10 g/L MWCNTs), and C (control; no MWCNTs) were examined at 200× magnification (excepted for the bottom right photo, which was 100× magnification) by light microscopy. (A) The three upper images show cultured cells in a sample from Group A. Free cells and cells interacting with MWCNTs (black clumps) are visible. (B) The middle (expanded) image shows cultured cells in a sample from Group B. (C) The bottom images show cultured cells in a sample from control Group C.

The reference materials, namely, carbon blacks have also shown some adverse effect; this, however, was smaller than MWCNTs. The cell density in Group R1 (carbon blacks, 0.05 g/l) and Group R2 (carbon blacks, 0.10 g/l) was 45 and 36 cell/1μl, respectively. On the other hand, for MWCNTs, the cell density was 38 and 27 cell/μl, respectively, under the identical situations. Very few black clumps (cells interacted with carbon black particles) were also observed, the percentage of the area of the cells covered by carbon blacks however, ranged from 0 to 20%.

In some sense, the cells in the aggregates played a protective role: Although some cells were sacrificed, their

RESEARCH ARTICLE

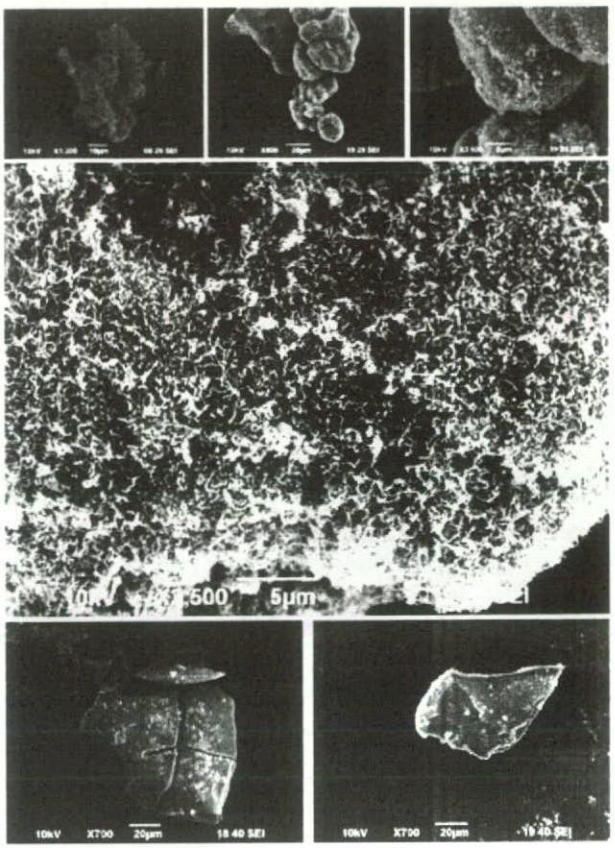

Fig. 2. Scanning electron microscopy was used to examine rice cells growing in the presence and absence of MWCNTs. (A) The three upper images and the middle (expanded) image show MWCNTs wrapped around rice cells, forming aggregates. (B) The bottom images show cells from control samples (Group C).

association with the MWCNTs made it less likely that other cells in the culture would interact with CNTs and also be precipitated. This effect can be viewed as a self-defense mechanism whereby a portion of the cell population is lost to save the rest of the culture from MWCNTs. It is known that plants have induced self-defense responses to a variety of biotic and abiotic stresses.[13–17] Biotic stresses include attack by herbivores and pathogens; abiotic stresses include factors such as atmospheric pollutants, light conditions, temperature variation, water availability, and salinity that can adversely affect plants. To protect themselves from stresses, plants can trigger the hypersensitive response, which results in the production of proteins or other organic chemicals that help them adapt to changes in the environment. For example, to protect themselves from viruses, plants create a zone of dead cells around an infection site that prevents the infection from spreading.[18]

The cell walls of plants are built up by harbor proteins and polysaccharides. It is possible that MWCNTs bind to certain proteins or polysaccharides, and that this binding causes a signaling cascade that results in strengthening of the cell walls due to increased production of proteins or polysaccharides. A recent study indicated that MWCNTs could alter protein expression in epithelial cells, which are the cells most affected by occupational exposure in nanotube manufacturing.[19] Another study used spectroscopic techniques to examine a composite formed by single walled carbon nanotubes and rice starch, and identified non-covalent interactions between the CNTs and the starch.[20] These two studies support the idea that CNTs can interact with certain proteins or polysaccharides. More experiments are needed to characterize the interaction between the cell wall and MWCNTs we observed in this study.

In conclusion, this study showed that rice cells can interact with MWCNTs in culture, and that this interaction results in a self-defense response by the rice cells. To the best of our knowledge, it is also the first study to investigate the possible impact of CNTs on plants. These preliminary experimental results show that MWCNTs pose a potential threat to rice at relatively high concentrations. Further studies will be needed to determine the impact of MWCNTs on rice growth and production.

Acknowledgments: This work was supported by funding from Grants-in-Aid for Scientific Research from the Ministry of Education, Culture, Sports, Science and Technology of Japan (No. 18310049), by the Japan Science and Technology Agency (JST), and by the Ministry of Health, Labor, and Welfare (No. H18-Chem-Gen-006).

References and Notes

1. P. Ball, Roll up for the revolution. *Nature* 414, 142 (2001).
2. H. Hyung, J. D. Fortner, J. B. Hughes, and J.-H. Kim, Natural organic matter stabilizes carbon nanotubes in the aqueous phase. *Environ. Sci. Technol.* 41, 179 (2007).
3. M. Bottini, et al., Multi-walled carbon nanotubes induce T lymphocyte apoptosis. *Toxicol. Lett.* 160, 121 (2006).
4. K. F. Soto, A. Carrasco, T. G. Powell, K. M. Garza, and L. E. Murr, Comparative in vitro cytotoxicity assessment of some manufactured nanoparticulate materials characterized by transmission electron microscopy. *J. Nanopart. Res.* 7, 145 (2005).
5. J. Muller, et al., Respiratory toxicity of multi-wall carbon nanotubes. *Toxicol. Appl. Pharmacl.* 207, 221 (2005).
6. G. Jia, et al., Cytotoxicity of carbon nanomaterials: Single-wall nanotube, multi-wall nanotube, and fullerene. *Environ. Sci. Technol.* 39, 1378 (2005).
7. D. B. Warheit, B. R. Laurence, K. L. Reed, D. H. Roach, G. A. Reynolds, and T. R. Webb, Comparative pulmonary toxicity assessment of single-wall carbon nanotubes in rats. *Toxicol. Sci.* 77, 117 (2004).
8. C. W. Lam, J. T. James, R. McCluskey, and R. L. Hunter, Pulmonary toxicity of single-wall carbon nanotubes in mice 7 and 90 days after intratracheal instillation. *Toxicol. Sci.* 77, 126 (2004).
9. N. A. Monteiro-Riviere, R. J. Nemanich, A. O. Inman, Y. Y. Wang, and J. E. Riviere, Multi-walled carbon nanotube interactions with human epidermal keratinocytes. *Toxicol. Lett.* 155, 377 (2005).
10. T. Murashige and F. Skoog, A revised medium for rapid growth and bioassays with tobacco tissue cultures. *Physiol. Plant* 15, 437 (1962).

11. K. Toriyama and K. Hinata, Cell suspension and protoplast culture in rice. *Plant Sci.* 41, 179 **(1985)**.
12. F. Tian, D. Cui, H. Schwarz, G. Estrada, and H. Kobayashi, Cytotoxicity of single-wll carbon nanotubes on human fibroblasts. *Toxicol. Vitro.* 20, 1202 **(2006)**.
13. J. Chen, E. Dawn, E. Hall, J. Murata, and V. De Luca, L-alanine induces programmed cell death in V labrusca cell suspension cultures. *Plant Sci.* 171, 734 **(2006)**.
14. D. Ren, K.-Y. Yang, G.-J. Li, Y. Liu, and S. Zhang, Activation of Ntf4, a tobacco mitogen-activated protein kinase, during plant defense response and its involvement in hypersensitive response-like cell death. *Plant Physiology* 141, 1482 **(2006)**.
15. H. Zhang, X. Zhang, Q. Li, and Z.-H. He, Alpha-picolinic acid activates diverse defense responses of salicylic acid-, jasmonic acid/ethylene- and Ca2+-dependent pathways in Arabidopsis and rice suspension cells. *Acta Botanica Sinica* 46, 1200 **(2004)**.
16. Y. Ichinose, S. Andi, R. Doi, R. Tanaka, F. Taguchi, M. Sasabe, K. Toyoda, T. Shiraishi, and T. Yamada, Generation of hydrogen peroxide is not required for harpin-induced apoptotic cell death in tobacco BY-2 cell suspension culture. *Plant Physiol. Biochem.* 39, 771 **(2001)**.
17. A. Cazalé, M. Rouet-Mayer, H. Barbier-Brygoo, Y. Mathieu, and C. Laurière, Oxidative burst and hypoosmotic stress in tobacco cell suspensions. *Plant Physiology* 116, 659 **(1998)**.
18. Y. Liu, M. Schiff, K. Czymmek, Z. Tallóczy, B. Levine, and S. P. Dinesh-Kumar1, Autophagy regulates programmed cell death during the plant innate immune response. *Cell* 121, 567 **(2005)**.
19. F. A. Witzmann and N. A. Monteiro-Riviere, Multi-walled carbon nanotube exposure alters protein expression in human keratinocytes. *Nanomedicine: Nanotechnolgy, Biology, and Medicine* 2, 158 **(2006)**.
20. A. Casey, G. F. Farrell, M. McNamara, H. J. Byrne, and G. Chambers, Interaction of carbon nanotubes with sugar complexs. *Synth. Met.* 153, 357 **(2005)**.

Received: 8 May 2007. Revised/Accepted: 12 June 2007.

Dental Materials Journal 2009; 28(1): 82–88

Original Paper

Development of a multiwalled carbon nanotube coated collagen dish

Michiko TERADA[1], Shigeaki ABE[2], Tsukasa AKASAKA[2], Motohiro UO[2], Yoshimasa KITAGAWA[1] and Fumio WATARI[2]

[1]*Oral Diagnosis and Oral Medicine, Department of Oral Pathobiological Science, Graduate School of Dental Medicine, Hokkaido University*
[2]*Department of Biomedical, Dental Materials and Engineering, Division of Oral Health Science, Graduate School of Dental Medicine, Hokkaido University, Kita-13, Nishi-7, Kitaku, Sapporo 060-8586, Japan*
Corresponding author, Michiko TERADA; E-mail: terada@den.hokudai.ac.jp

Carbon nanotubes (CNTs) are one of the most interesting nanomaterials because of their excellent characteristics. In this study, a transparent CNTs coating for cell culture dishes was developed and its properties for cell culture were estimated. Carboxylated multiwalled carbon nanotubes (MWCNTs) were dispersed in aqueous sodium cholate solution and applied on a collagen type I-coated cell culture dish (cover glass). The dish surface was homogeneously covered by MWCNTs without aggregation. The MWCNT-coated dish was slightly gray and had good transparency, so conventional optical microscopic observation of the cells on the MWCNT-coated dish was possible. Rat osteoblast-like cells cultured on the MWCNT-coated dish showed slightly lower viability and proliferation compared to the collagen-coated dish. The cell adhesion on the MWCNT-coated dish was much higher than that on the collagen-coated dish. Therefore, MWCNT-coating for dishes will be a useful new material for cell culture.

Key words: Multiwalled carbon nanotubes (MWCNTs), Collagen, Cell culture

Received May 1, 2008: Accepted Jul 25, 2008

INTRODUCTION

Carbon nanotubes (CNTs) and other carbon nanomaterials are of interest for biological and medical applications because of their high chemical durability, mechanical strength and electrical properties. Studies of the application of carbon nanomaterials have been carried for the substrate of cell culture[1-9], drug delivery systems[10,11] and medical implant materials[12,13].

Cells have high affinity to singlewalled CNTs (SWCNTs)[5-7,9,14], multiwalled CNTs (MWCNTs)[2,4,6-8] and other carbon nanofibers[1-3]. The bone cell affinity to CNTs[1,14] and bone formation (osseointegration) on sintered MWCNTs were reported[12]. However, those CNT-based substrates were black and had low optical transparency. Therefore, conventional optical microscopic observation of the cultured cells on the CNT-based substrates was quite difficult and the cells needed to be observed by scanning electron microscopy (SEM) after fixation. However, *in situ* microscopic observation of cultured cells on CNTs is important to evaluate the cell affinity to them.

MacDonald *et al.* reported a collagen-SWCNT composite for the cell culture substrate[5]. The SWCNTs were strongly entrapped by collagen and the composite showed high mechanical strength and good cell viability. Then good affinity between collagen and CNTs was expected.

On the other hand, collagen is one of the most biocompatible materials, and then collagen-coated dish is widely used for cell culture. From the Macdonald's result, CNTs would show high affinity to the collagen-coated dish surface. Then above CNTs remarkable properties would be added to the collagen-coated dish. Concerning to the CNTs, purification and surface treatment was easier carried out for MWCNTs than SWCNTs because of their chemical stability resulted from thick tubular structure. Thus MWCNTs coating on the collagen-coated dish would be possible by the appropriate treatment of MWCNTs.

In this study, MWCNTs were coated onto collagen-coated cell culture, in an attempt to develop coated dishes with optically transparent MWCNTs, and the cell viability, proliferation, and adhesion on the MWCNT-coated dishes were estimated.

MATERIAL AND METHODS

Preparation of MWCNT-coated dishes and surface roughness measurement

MWCNTs (20-30nm in diameter, Cnt, Seoul, Korea) were purified by oxidation at 500°C for 90 minutes and treated in concentrated hydrochloric acid. The purified MWCNTs were carboxylated by the method reported by Peng *et al.*[15] to improve their dispersion in aqueous solutions. The carboxylated MWCNTs were dispersed in sodium cholate (1w/v%) aqueous solution to MWCNT concentrations of 1-1,000ppm under sonication for 90 minutes. Sodium cholate was reported to be one of the most effective surfactants

for carbon nanotube dispersion[16]. The obtained MWCNT suspension (2ml/dish) was poured into a collagen type I-coated cell culture dish (35mm ϕ, Iwaki, Tokyo, Japan) and kept at room temperature for 3 hours. Then it was rinsed with deionized water, dried and employed for the following cell culture experiments. For the SEM observations, a collagen type I coated cover glass (25mm ϕ, Iwaki, Tokyo, Japan) with the same treatment was used instead of the culture dish. Hereafter, the dishes and the cover glasses treated with the MWCNT suspension are referred to as "MWCNT-coated dish" and "MWCNT-coated cover glass", respectively.

To estimate the optimum treatment conditions for the MWCNT solution, the collagen-coated dishes were treated with 1-1,000ppm suspensions in 1w/v% sodium cholate aqueous solution for 1-6 hours. The homogeneity of the MWCNT coating on these dishes was estimated by SEM observation (S-4000, Hitachi, Japan) and optimum treatment conditions were determined. The changes in surface roughness of the collagen-coated cover glass before and after MWCNT coating were estimated using a surface roughness meter (Surfcom 130A, Tokyo Seimitsu, Tokyo, Japan).

Cell prolification, viability and adhesion on MWCNT-coated dishes

Rat osteoblast-like MC3T3-E1 cells were seeded onto MWCNT-coated dishes and collagen-coated dishes at 1×10^5cells/2ml/dish. These cells were cultured in α-MEM (Gibco, USA) with 10% FBS (Biowest, USA) and PSN Antibiotic Mixture (Gibco, USA) at 37°C in humidified 5% CO_2 for 24, 48 and 72 hours and used for the following proliferation and viability estimations. Observation and cell counting were done under an optical microscope after fixation and Giemsa staining (Merck, USA). The number of cells per dish was estimated under optical microscopic observation and the cell proliferation was estimated. Cell viability was measured by colorimetry using Alamer blue (Biosource, USA). The cells were cultured in medium containing 10% Alamer blue and the changes in absorbance at 570nm and 600nm were estimated using a spectrophotometer (U-1100, Hitachi, Japan). Cell adhesion was estimated by treatment using diluted Trypsin-EDTA solution (Gibco, USA). The MC3T3-E1 cells that were cultured to confluence on MWCNT-coated dishes and collagen-coated dishes were treated with 0.1% and 0.02% Trypsin-EDTA solution. The decrease of the attached cells with treatment time was evaluated under an optical microscope.

RESULTS

Fig. 1 shows SEM images of MWCNT-coated cover glasses treated with various concentrations of

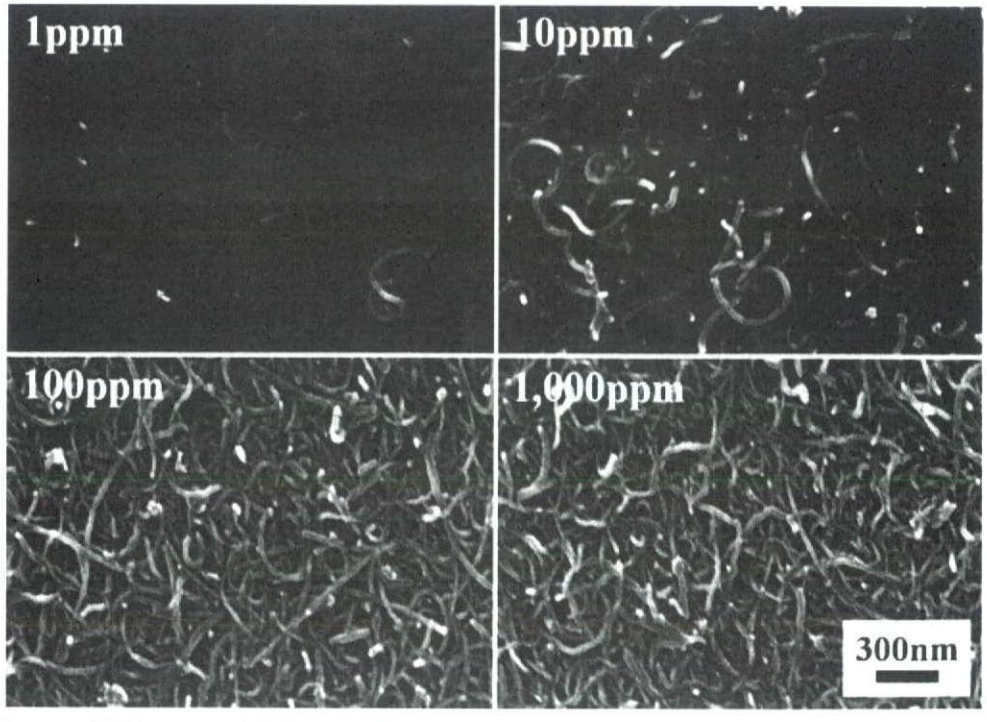

Fig. 1 SEM images of MWCNT adhering to collagen-coated cover glass treated with MWCNT suspensions at the concentrations of 1, 10, 100 and 1,000ppm for 3 hours.

carboxylated MWCNT suspension. The coverage of MWCNTs on the surface was increased with the increase of the MWCNT concentration from 10ppm to 1,000ppm. In contrast, MWCNT aggregation was observed on the dish treated with 1,000ppm MWCNT suspension. Therefore, the optimum concentration of the MWCNT suspension for the coating treatment was estimated to be 100ppm. The effect of the treatment period using 100ppm suspension was also estimated and optimum MWCNT coverage was obtained after 3-hour treatment.

No significant difference was observed in the arithmetic mean surface roughness (Ra) of the collagen- and MWCNT-coated cover glass because of the detection limit. The maximum roughness (Rmax) of the MWCNT-coated cover glass was estimated to be 0.78 ± 0.08 μm and it was slightly higher than that of the collagen-coated cover glass (Rmax=0.52 ± 0.05 μm). Thus the MWCNT-coated surface was estimated to be as smooth as the collagen-coated surface.

The MWCNT-coated dishes used in the following experiments were treated with 100ppm MWCNT suspension for 3 hours. The MWCNTs were strongly entrapped on the collagen-coated surface and never released by rinsing or cell culture procedures.

Fig. 2 shows a comparison of the color and the transparency of the collagen-coated dish and the MWCNT-coated dish. The MWCNT-coated dish looked slightly gray but had good transparency.

Fig. 3 shows the cell proliferation on an MWCNT-coated dish and collagen-coated dish. The cells on both dishes showed similar tendencies and their difference was not significant until 48 hours (t-test, $p<0.05$). Fig. 4 shows cell viability on both dishes. The cell viability on the MWCNT-coated dish was slightly lower than that on the collagen-coated dish.

Fig. 5 shows optical microscope images (a) and SEM images (b) of the cultured cells on MWCNT-coated and collagen-coated dishes. The changes in cell morphology on both dishes were similar in the optical images; however, the cells on the MWCNT-coated dish were not widespread as those on the collagen-coated dish. Fig. 6 shows high magnification SEM images of the filopodia of E1 cells. Large numbers of filopodia were observed in the cells on the MWCNT-coated dish and the ends of the filopodia appeared to contact MWCNTs.

Fig. 7 shows the residual cell percentage of the dish surface in the Trypsin-EDTA treatment period (values represent mean detachment of cells ± SD from n=4.). Cells on the MWCNT-coated dish were

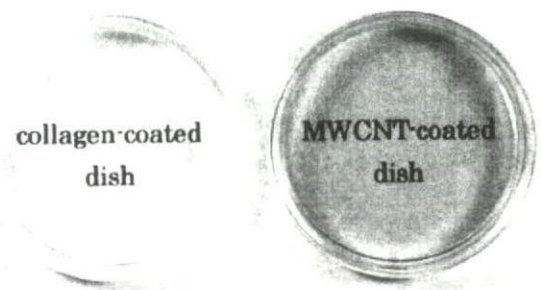

Fig. 2 Transparency of the MWCNT- and collagen-coated dishes

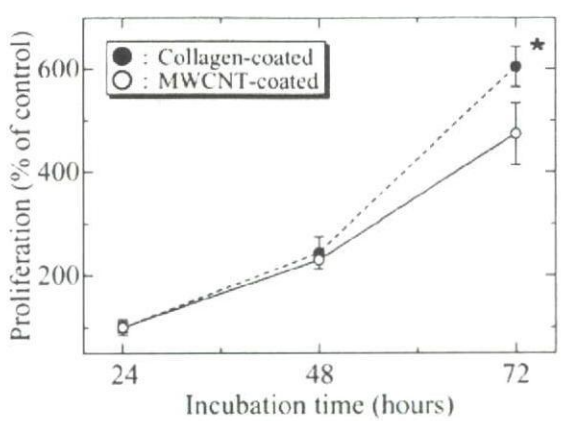

Fig. 3 Quantification of MC3T3-E1 cell growth on an MWCNT-coated dish Values represent mean cell counts ±SD from n=6 fields of observation per treatment; *, $p<0.05$ compared with MWCNT-coated dish at 72 hours.

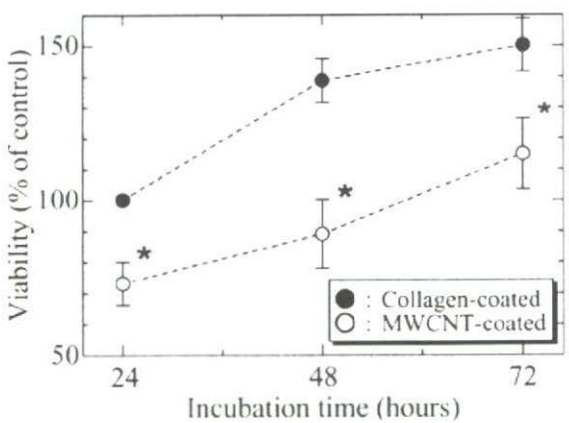

Fig. 4 Viability of MC3T3-E1 cells cultured on the MWCNT- and collagen-coated dishes.
Values represent mean cell viability ±SD from n=5; *, $p<0.05$ compared with collagen-coated dish.

detached from the dish surface within a few minutes with 0.1% Trypsin-EDTA solution. Even with the lower concentration of Trypsin-EDTA (0.02%), all cells on the collagen-coated dish were detached within 10 minutes. In contrast, some of the cells on the MWCNT-coated dish remained on the surfaces of MWCNTs for more than 30 minutes of 0.1% Trypsin-EDTA treatment. Fig. 8 shows that cells were detached with 0.02% Trypsin-EDTA solution at 2 minutes. Fig. 9 shows SEM images of the cells on an MWCNT-coated dish after 2 minutes of treatment with 0.02% Trypsin-EDTA solution. Mechanical contact between the filopodia and MWCNTs could be observed.

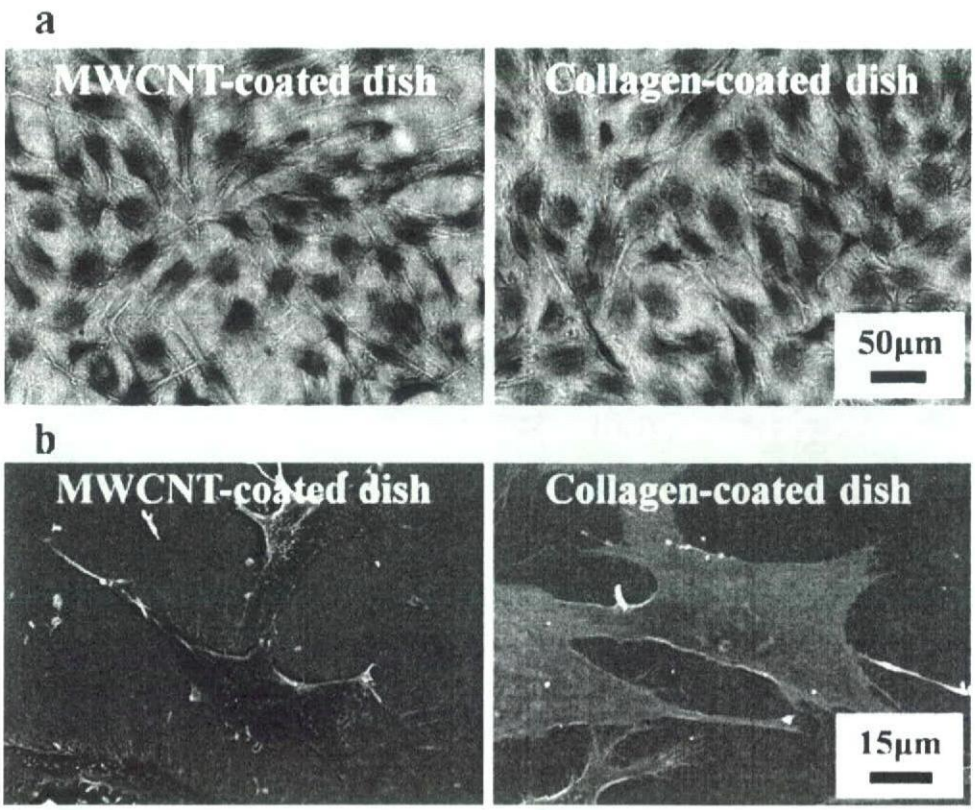

Fig. 5 (a) Optical microscope image of MC3T3-E1 cells on the surface of collagen-and MWCNT-coated dishes.
(b) Low magnification SEM image of MC3T3-E1 cells on the surface of collagen- and MWCNT-coated dishes.

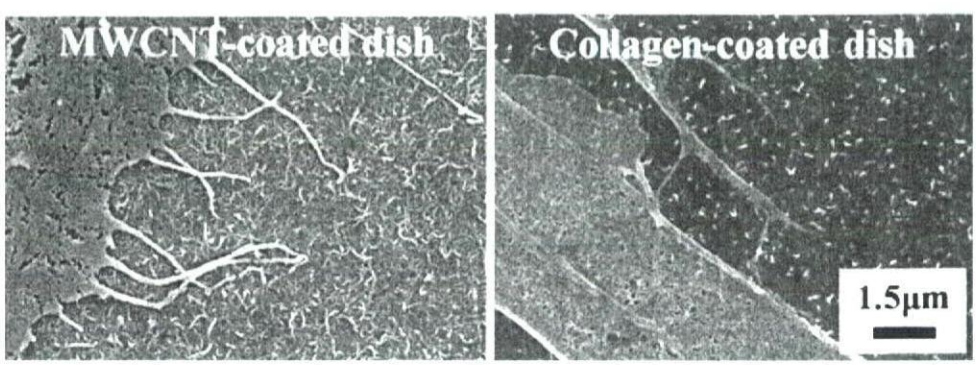

Fig. 6 High magnification SEM images of MC3T3-E1 cells on the surface of the collagen- and MWCNT-coated dishes.

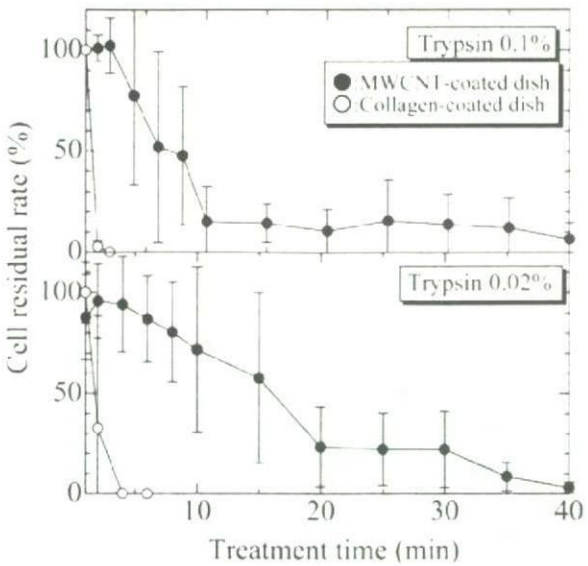

Fig. 7 Cell attachment test
○: Collagen-coated dish, ●: MWCNT-coated dish.

DISCUSSION

Usually, CNTs and other carbon nanoparticles have low dispersion in aqueous solutions because of their hydrophobicity. However purification and surface treated methods were well studied for MWCNTs than SWCNTs, and carboxylated MWCNTs[15] can be stably dispersed into sodium cholate aqueous solution[16]. The collagen-coated dishes could be homogeneously covered by MWCNTs using the above suspension, as shown in Fig. 1, under optimum treatment conditions (100ppm for 3 hours). SEM and surface roughness observations revealed that the collagen-coated surface was homogeneously and fully covered with MWCNTs without their aggregation. The carboxylation of MWCNTs and sodium cholate addition were effective to obtain homogeneous coverage of MWCNTs on the collagen-coated dish surface.

Concerning to the interaction between CNTs and collagen, MacDonald *et al.*[5] reported SWCNT-

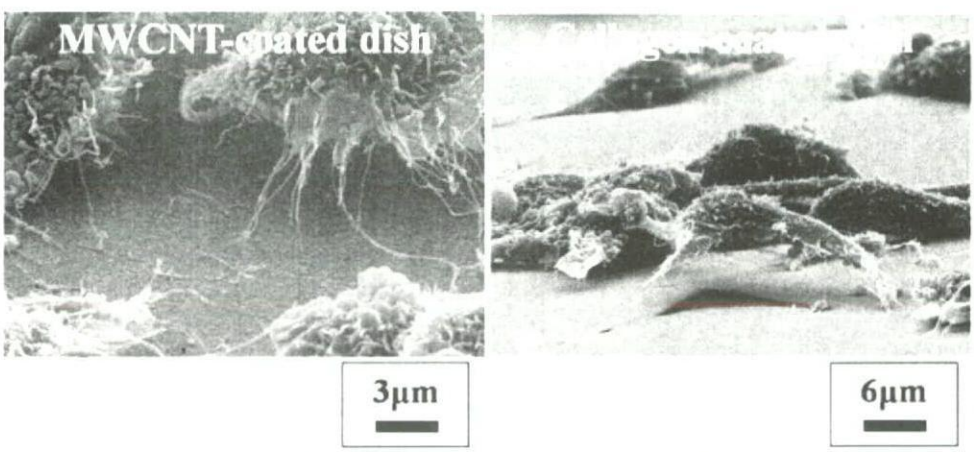

Fig. 8 SEM images of MC3T3-E1 cells treated with 0.02% Trypsin-EDTA for 1 to 2 minutes on the surface of a collagen- and MWCNTs-coated dish.

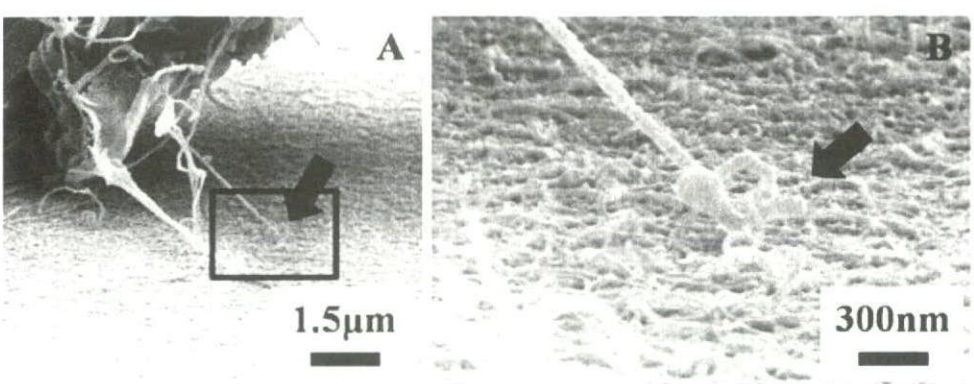

Fig. 9 SEM images of mechanical coupling of filopodia on an MWCNT-coated dish
A: low magnification view, B: enlargement of the square in A.
The arrow: mechanical coupling between filopodia and MWCNTs.

reinforced collagen. As the mechanism of SWCNT entrapment in collagen, they suggested the blend and interaction between CNTs and collagen fibrils. In the present study, MWCNTs were homogeneously coated on collagen-coated cell culture dishes and cover glass. The coated MWCNTs were strongly fixed on the collagen-coated surface. Thus, strong entrapment of MWCNTs by collagen would also have occurred via a similar mechanism

The prepared MWCNT-coated dishes showed good transparency and conventional optical microscopic observation could be easily carried out. Usually, cell culture studies on CNTs were carried out on the CNTs membranes which have no optical transparency. Therefore the observation of cells on CNT membranes should be carried out by SEM. Our MWCNT-coated dishes had a densely packed MWCNT surface with optical transparency, and optical microscopic observation of cells cultured on MWCNTs became possible. Thus, they would be suitable MWCNT substrate for cell culture study on MWCNTs.

The proliferation and viability of the cells on the MWCNT-coated dish were slightly lower than those on the collagen-coated dish as shown in Fig. 3 and Fig. 4. In addition, the cells on the MWCNT-coated dish were widely extended on that dish surface (Fig. 5). The cell adhesion on the MWCNT-coated dish was quite strong as shown in Fig. 7. Aoki *et al.*[8] reported that the cells on an MWCNT membrane were strongly attached and were not detached by trypsin treatment. That was in good agreement with our results. As shown in Fig. 9, mechanical contact between MWCNTs and pseudopods of the cells was observed. Aoki *et al.*[8] and Zanello *et al.*[14] also reported the same mechanical contact of bone cells cultured on MWCNTs. This mechanical binding would be one reason for the high adhesion, and the large specific surface area of MWCNTs would also be effective to increase the adhesion.

There were many reports of the interaction between SWCNTs and MWCNTs and variety of cells. Hu *et al.*[9] reported good neural cell viability on MWCNTs deposited on the polyethyleneimine-coated cover glass. Aoki *et al.*[8] and Zanello *et al.*[14] reported the comparison of bone cell proliferation on various CNTs. Aoki *et al.*[7] found the highest cell proliferation and viability on the SWCNT membranes. Those for MWCNTs were lower than for SWCNTs but higher than for graphite particles. Zanello *et al.*[14] also reported higher cell proliferation on SWCNTs than on MWCNTs, but the osteoblasts cultured on MWCNTs showed an osteocyte-like shape. That suggested the differentiation of osteoblasts on MWCNTs. Thus the interaction between various cells and CNTs was strongly interested. However, most of CNTs substrates had no optical transparency, and then cell observation should be carried with SEM. This means the difficulty of the conventional cell observation *in situ* with optical microscope while cell cultured. Our aim was to prepare the CNTs based cell culture substrate which is applicable for ordinary cell culture and optical microscope observation. The obtained MWCNT-coated dish in this study had densely MWCNT-coated surface with good optical transparency. Then, cell morphology and behavior on MWCNTs while cultivation could be observed with optical microscope *in situ*. The cell proliferation and viability of the cells on those dish was comparable to those of the collagen-coated dish which is known as the one of the best substrate for cell culture. In addition, cell adhesion on the MWCNT-coated dish was extremely stronger than the collagen-coated dish. The preparation of the present MWCNT-coated cell culture materials was quite simple and it would be applicable for other carbon nanomaterials e.g. SWCNTs or carbon nanohornes. Thus, the feasibility of the MWCNT-coated dish for the application of cell culture on the MWCNTs and other carbon nanomaterials was suggested.

The MWCNT-coated dish prepared in the present study would provide cell proliferation and viability of the cells comparable to those of the collagen-coated dish. And cell adhesion on the MWCNT-coated dish was extremely stronger than the collagen-coated dish. The collagen-coated dish is one of the best substrates for cell culture. The preparation of the present MWCNT-coated cell culture materials was quite simple and showed good transparency. Thus, the feasibility of the MWCNT-coated dish for cell culture was suggested.

CONCLUSION

Carboxylated MWCNTs were homogeneously coated on collagen-coated cell culture dishes. The MWCNTs were strongly entrapped on the collagen-coated dish surface and the dishes had good optical transparency. Thus, *in situ* optical microscope observation of cultured cells on the MWCNTs was possible. The viability and proliferation of MC3T3-E1 cells on MWCNT-coated dishes were comparable to those on dishes coated with collagen, which is one of the most appropriate substrates for cell culture. The MWCNT-coated dishes had high cell viability comparable to that on collagen-coated dishes, and the cell adhesion on the MWCNT-coated dishes was quite strong compared to that on the collagen-coated dishes. SEM images suggested that one of the reasons for the strong cell adhesion on MWCNT-coated dishes was the mechanical contact between MWCNTs and pseudopods. Therefore, the coating of carboxylated MWCNTs on collagen-coated dishes will be useful not only for *in situ* cell observation on CNTs but also for

the improvement of cell adhesion.

ACKNOWLEDGMENTS

This work was supported by Research on Advanced Medical Technology in Health and Labour Sciences Research Grants from the Ministry of Health, Labour and Welfare of Japan.

REFERENCES

1) Price RL, Waid MC, Haberstroh KM, Webster TJ. Selective bone cell adhesion on formulations containing carbon nanofibers. Biomaterials 2003; 24: 1877-1887.
2) Hu H, Ni Y, Montana V, Haddon RC, Parpura V. Chemically functionalized carbon nanotubes as substrates for neuronal growth. Nano Lett. 2004; 4: 507-511.
3) McKenzie JL, Waid MC, Shi R, Webster TJ. Decreased functions of astrocytes on carbon nanofiber materials. Biomaterials 2004; 25: 1309-1317.
4) Correa-Duarte MA, Wagner N, Rojas-Chapana J, Morsczeck C, Thie M, Giersing M. Fabrication and biocompatibility of carbon nanotube-based 3D networks as scaffolds for cell seeding and growth. Nano Lett. 2004; 4: 2233-2236.
5) MacDonald RA, Laurenzi BF, Viswanathan G, Ajayan PM, Stegemann JP. Collagen-carbon nanotube composite materials as scaffolds in tissue engineering. J. Biomed. Mater. Res., Part A 2005; 74A: 489-496.
6) Hu H, Ni Y, Mandal SK, Montana V, Zhao B, Haddon RC, Parpura V. Polyethyleneimine functionalized single-walled carbon nanotubes as a substrate for neuronal growth. J. Phys. Chem. B 2005; 109: 4285-4289.
7) Aoki N, Akasaka T, Watari F, Yokoyama A. Carbon nanotubes as scaffolds for cell culture and effect on celular functions. Dent. Mater. J. 2007; 26: 178-185.
8) Aoki N, Akasaka T, Yokoyama A, Nodasaka Y, Akasaka T, Uo M, Sato Y, Thoji K, Watari F. Cell culture on a carbon nanotube scaffold. J. Biomed. Nanotechnol. 2005; 1: 402-405.
9) Jan E, Kotov NA. Successful differentiation of mouse neural stem cells on layer-by-layer assembled single-walled carbon nanotube composite. Nano Lett. 2007; 7: 1123-1128.
10) Ajima K, Yudasaka M, Maigné A, Miyawaki J, Iijima S. Effect of functional groups at hole edges on cisplatin release from inside single-wall carbon nanohorns. J. Phys. Chem. B 2006; 110: 5773-5778.
11) Feazell RP, Nakayama-Ratchford N, Dai H, Lippard SJ. Soluble single-walled carbon nanotubes as longboat delivery systems for platinum (IV) anticancer drug design. J. Am. Chem. Soc. 2007; 129: 8438-8439.
12) Wang W, Watari F, Omori M, Liao S, Zhu Y, Yokoyama A, Uo M, Kimura H, Ohkubo A. Mechanical properties and biological behavior of carbon nanotube/polycarbosilane composites for implant materials. J. Biomed. Res., Part B 2007; 82B: 223-230.
13) Usui Y, Aoki K, Narita N, Murakami N, Nakamura I, Nakamura K, Ishigaki N, Yamazaki H, Horiuchi H, Kato H, Taruta S, Kim YA, Endo M, Saito N. Carbon nanotubes with high bone-tissue compatibility and bone-formation acceleration effects. Small 2008; 4: 240-246.
14) Zanello LP, Zhao B, Hu H, Haddon RC. Bone cell proliferation on carbon nanotubes. Nano Lett. 2006; 6: 562-567.
15) Peng H, Alemany LB, Margrave JL, Khabashesku VN. Sidewall carboxylic acid functionalization of single-walled carbon nanotubes. J. Am. Chem. Soc. 2003; 125: 15174-15182.
16) Ishibashi A, Nakashima N. Individual dissolution of single-walled carbon nanotubes in aqueous solutions of steroid or sugar compounds and their roman and near-ir spectral properties. Chem. --Eur. J. 2006; 12: 7595-7602.

X-ray absorption fine structure (XAFS) analyses of Ni species trapped in graphene sheet of carbon nanofibers

Mayuko Ushiro, Kanae Uno, and Takashi Fujikawa*
Graduate School for Science, Chiba University, Yayoi-cho 1-33, Inage-ku, Chiba 263-8522, Japan

Yoshinori Sato and Kazuyuki Tohji
Graduate School of Environmental Studies, Tohoku University, Aoba, Sendai 980-8579, Japan

Fumio Watari
Graduate School of Dental Medicine, Department of Biomedical, Dental Materials and Engineering, Hokkaido University, Kita 13 Nishi 7, Sapporo, 060-8586, Japan

Wang-Jae Chun
Catalysis Research Center, Hokkaido University and Core Research for Evolution Science and Technology, Japan Science and Technology Corporation, Kita 21 Nishi 11, Sapporo, 001-0021, Japan

Yuichiro Koike and Kiyotaka Asakura
Catalysis Research Center, Department of Quantum Science and Engineering, Hokkaido University, Kita 21 Nishi 11, Sapporo, 001-0021, Japan

(Received 28 October 2005; revised manuscript received 28 December 2005; published 10 April 2006)

Metal impurities in the carbon nanotubes and carbon nanofibers play an important role in understanding their physical and chemical properties. We apply the Ni *K*-edge x-ray absorption fine structure analyses to the local electronic and geometric structures around embedded Ni impurities used as catalysts in a carbon nanofiber in combination with multiple scattering analyses. We find almost Ni catalysts as metal particles are removed by the purification treatment. Even after the purification, residual 100 ppm Ni species are still absorbed; most of them are in monomer structure with Ni-C bond length 1.83 Å, and each of them is substituted for a carbon atom in a graphene sheet.

DOI: 10.1103/PhysRevB.73.144103 PACS number(s): 61.10.Ht, 87.64.Fb, 87.64.Gb, 61.46.−w

I. INTRODUCTION

Carbon nanotubes (CNTs)[1,2] and carbon nanofibers (CNFs)[3,4] are promising nano materials for electric devices, hydrogen reservoir, reinforce composites, medical usages and so on. There are several preparation methods to produce CNTs/CNFs, where the metal catalysts play a decisive role in their production processes. Although most of them can be removed from the CNTs/CNFs by acid treatments,[5] a small amount of impurities are left in the CNTs/CNFs after the purification processes.[6] The metals are intimately associated with the nanotube samples.[6] These impurities are reported to affect a giant thermopower due to a Kondo effect,[7] quantum conductance,[8] and anomalous temperature dependence of the resistivity.[9] In addition to the modification of the physical properties of CNTs/CNFs some metals such as Ni show biotoxic effects on a human body when they are used in medical applications such as drag delivery systems, medical implants and scaffolds.[10–12] In order to understand the effect of metal atoms on the physical properties as well as the removal of these impurities, the structure of metal species left in the CNT will be important. Furthermore the knowledge about the local structure will provide a hint to the formation mechanism for the CNTs/CNFs.

From these standpoints of view the structures of metal species trapped in CNTs and CNFs have intensively been discussed theoretically. Several adsorption sites and model structures are proposed such as adsorption on Stone-Wales defects,[13] monomer or dimer adsorption model on the graphene sheet,[14] metal adsorption on atop of C atom[9,15] or on axial C-C bond,[16] a substitutional site of graphene sheet.[17,18] Lee *et al.* propose Ni-C σ bond is formed during the catalytic formation reaction of a single wall CNT and a Ni may be trapped at a substitutional position in the CNT wall.[19] However, we have had no definite conclusion for the location of metal atoms due to the lack of direct experimental evidence about the local structure around the metal impurities.

Recently Asakura *et al.* reported a letter concerning extended x-ray absorption fine structure (EXAFS) studies on the structure of Ni impurities left in a CNF after the purification.[20] Ni is one of the important catalyst to prepare CNTs and CNFs. They concluded that the dimer species were embedded in the CNFs with covalent Ni-C bonds. However, there are two criticisms on their conclusions.

(1) Where are these Ni atoms located?

(2) Are they really in dimers?

The first question comes from the fact that EXAFS is a one-dimensional local structure analysis sensitive to the short range order around the metal within about 3 Å. The second question arises based on the Ni-Ni distance 2.48 Å found in the EXAFS analysis, the distance is almost equal to that of Ni foil. The Ni-Ni bonds they observed could be due to those

of trace amount of Ni particles left after the purification.

X-ray absorption near edge structure (XANES) spectra provide longer range information (typically ≈5 Å) than EXAFS spectra, and stereochemical information.[21,22] Although XANES contains more information than EXAFS,[22] XANES analysis is difficult because it requires multiple scattering calculations. Hence, XANES has often been used as a fingerprint by comparing it with those of reference compounds. Fujikawa *et al.* have developed a reliable XANES theory based on the short range order full multiple scattering approach.[23] They have successfully determined several material structures by simulating XANES spectra.[24–28] Asakura *et al.* have measured the XANES spectra of these species and have observed prominent spectral features after the purification. The spectral features are different from those found in Ni foil or Ni oxide, and are characteristic of Ni species in CNFs after the purification treatment. The detailed XANES analyses will provide important information about the above criticisms.

In this paper we report x-ray absorption fine structure (XAFS) analyses on the local structures around Ni in a CNF. First we describe EXAFS analyses of the Ni residue involved in a CNF before and after the purification in details. Second we explain the XANES analyses and investigate plausible structures. We find Ni atoms substitute carbon atoms in the CNF framework. Finally we compare the present result with the previous theoretical works, and discuss the merits of XANES in the material science.

II. EXPERIMENT

CNF is synthesized by a CVD method using Ni catalyst following a previous literature.[29] The CNF used here is hat-stacked carbon nanofiber (HSCNF) that is composed of graphene hats stacked toward the needle axis.[12] The diameter and the length of the CNF is 25–100 nm and 0.1–5.0 μm, respectively. It is purified by a calcination in atmosphere followed by 6.0 M HCl treatment for 6 hours in order to remove the carbon nanoparticles and Ni catalysts.

XAFS measurements are carried out at the BL9A in the Institute for Structure Material Science's Photon Factory (KEK-PF) using a Si(111) double crystal monochromator (99G280, 2001G117, and 2003G2477). A pair of bent conical

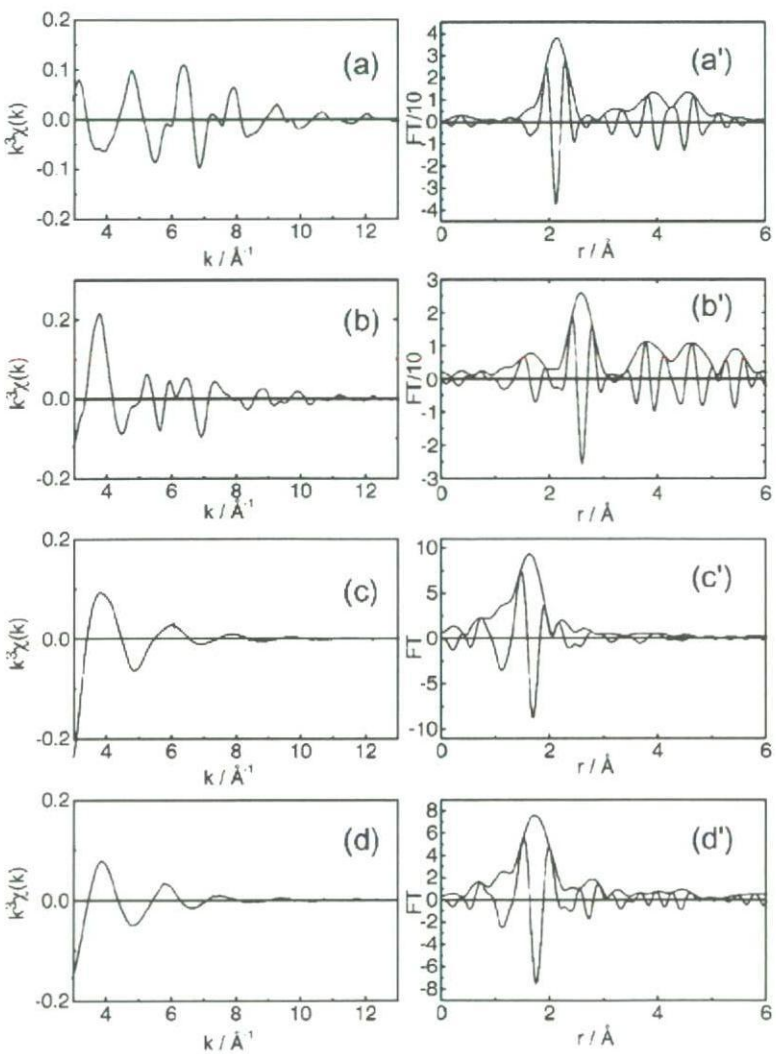

FIG. 1. Ni *K*-edge EXAFS oscillations (x) (x=a,b,c,d) and their Fourier transforms (x') (x'=a′,b′,c′,d′) of reference compounds: (a) (a′) Ni foil, (b) (b′) NiO, (c) (c′) $Ni(H_2O)_6(NO_3)_2$, and (d) (d′) $Ni(cp)_2$.

TABLE I. Curve fitting results for reference compounds. r is the distance to the neighbor, σ is the Debye-Waller factor, ΔE is a shift in edge energy, R is R-factor defined by Eq. (1), S is an amplitude reduction factor.

Sample	Bond	N	r/Å	$\sigma/10^{-2}$ Å	ΔE/eV	R/%	S
Ni foil	Ni-Ni	9.7±1.2 12[a]	2.47±0.02 2.49[a]	7.1±2.0	−11±5	1.0	0.80±0.1
NiO	Ni-O	5.8±0.4 6[a]	2.07±0.01 2.084[a]	8.0±1.0	−4.8±5	0.7	0.93±0.06 (Ref. 53)
	Ni-Ni	12.4±1.0 12[a]	2.95±0.02 2.954[a]	8.1±1.0	−3.5±3		1.0±0.1 (Ref. 53)
$Ni(H_2O)_6(NO_3)_2$	Ni-O	6.2±0.4 6[a]	2.04±0.01 2.063[a]	8.0±0.9	−2.0±1.0	3.5	1.0±0.1 (Ref. 54)
$Ni(C_5H_5)_2$	Ni-C	10.8±1.2 10[a]	2.17±0.01 2.196[a]	8.6±1.0	−5.7±3.0	3.0	1.1±0.1 (Ref. 55)

[a]The diffraction data.

mirrors focus the x-ray beam on the sample and remove higher harmonics.[30] The incident and transmitted x rays are monitored by ionization chambers filled with nitrogen. The fluorescence x rays are detected by a 19 element SSD (Solid State Detector, Camberra Co.). The dead times of SSD are corrected according to the literature.[31] The XAFS analyses are carried out by REX2000 (Rigaku Co.)[32,33] using phase shift and amplitude functions obtained from FEFF8.[21] The Fourier transformation of k^3-weighted $\chi(k)$ is carried out over the range $k=3-13$ Å^{-1}. The peaks are Fourier filtered with $\Delta r=1.2-2.2$ Å for the first shell with a Hamming window function, and the curve fitting analyses are carried out in the k-space. The goodness of fit is estimated by use of the R-factor defined by

$$R(\%)=\frac{\sum[k^3\chi_o(k)-k^3\chi_c(k)]^2}{\sum[k^3\chi_o(k)]^2}\times 100, \tag{1}$$

where χ_o and χ_c are the observed and the calculated fitting EXAFS oscillations.

III. THEORY

The XANES theory used in this paper is based on the short-range-order full multiple scattering theory proposed by Fujikawa *et al.*[34] Later, this theory was modified by a partitioning technique in order to reduce the computation time.[23,35–37] Here, we summarize the theoretical methods.

The x-ray absorption intensity σ from the core orbital $\phi_c(\mathbf{r})=R_{l_c}(r)Y_{L_c}(\hat{\mathbf{r}})$, $L_c=(l_c,m_c)$ at site A (x-ray absorbing atom) is given by Eq. (2) for photoelectron kinetic energy $\epsilon_k=k^2/2$. We assume excitation by a linearly polarized x ray in the z direction,[23]

$$\sigma=-\frac{8}{3}\mathrm{Im}\Bigg(\sum_{L,L',L_c} i^{l-l'}\exp[i(\delta_l^A+\delta_{l'}^A)]\rho_c(l)\rho_c(l') \times G(L_c 10|L)G(L_c 10|L')(t^{-1})_{LL}^{AA}[(1-X)^{-1}]_{LL'}^{AA}\Bigg), \tag{2}$$

where $G(LL'|L'')$ is Gaunt's integral and $\rho_c(l)$ is the radial dipole integral between the radial part of $\phi_c(\mathbf{r})$ and the lth partial wave of photoelectrons $R_l(r)$ at site A. The phase shift of the lth partial wave at site A is represented by δ_l^A. We introduce the matrix X specified with site index α and angular momentum L and so on; it is defined as

$$X_{LL'}^{\alpha\beta}=t_l^{\alpha}G_{LL'}(\mathbf{R}_\alpha-\mathbf{R}_\beta)(1-\delta_{\alpha\beta}), \tag{3}$$

where t_l^{α} and $G_{LL'}$ represent the T-matrix at site α and the Green's function in an angular momentum representation. The inverse matrix $(1-X)^{-1}$ includes an infinite order of the full multiple scattering inside the cluster we are considering. The phase shifts in $t_l^{\alpha}\{=-[\exp(2i\delta_l^{\alpha})-1]/2ik\}$ are one of the most important features and reflect the electronic structure of the surrounding atoms, which are calculated within the Hartree-Fock approximation. The Green's function $G_{LL'}$ reflects the geometrical structure. The clusters used in the present work include all surrounding atoms up to about 5 Å for the carbide model and about 7 Å for other models around an x-ray absorption atom.

IV. RESULTS AND DISCUSSION

A. EXAFS

We measure the x-ray spectra of Ni foil, NiO, $Ni(H_2O)_6(NO_3)_2$, $Ni(cp)_2$ (cp=cyclopentadienyl), as reference compounds whose EXAFS oscillations and Fourier transforms are given in Fig. 1. We carry out curve fitting analyses to check the validity of FEFF calculations and to obtain the correction parameters, S, for coordination numbers. The results are summarized in Table I: The curve fitting analyses can provide 0.02 Å accuracy in the bond length. The coordination numbers are a little scattered but the reduction factor S can be determined within 10% precision. We obtain the averaged reduction factors $S=0.9\pm0.1$ for Ni-Ni, and $S=1.0\pm0.1$ for Ni-C and Ni-O.

Figure 2 shows the observed Ni K-edge EXAFS spectra, their Fourier transforms and curve fitting results of Ni in the CNFs before and after the purification. Before the purification, the EXAFS oscillation is found to be similar to that of

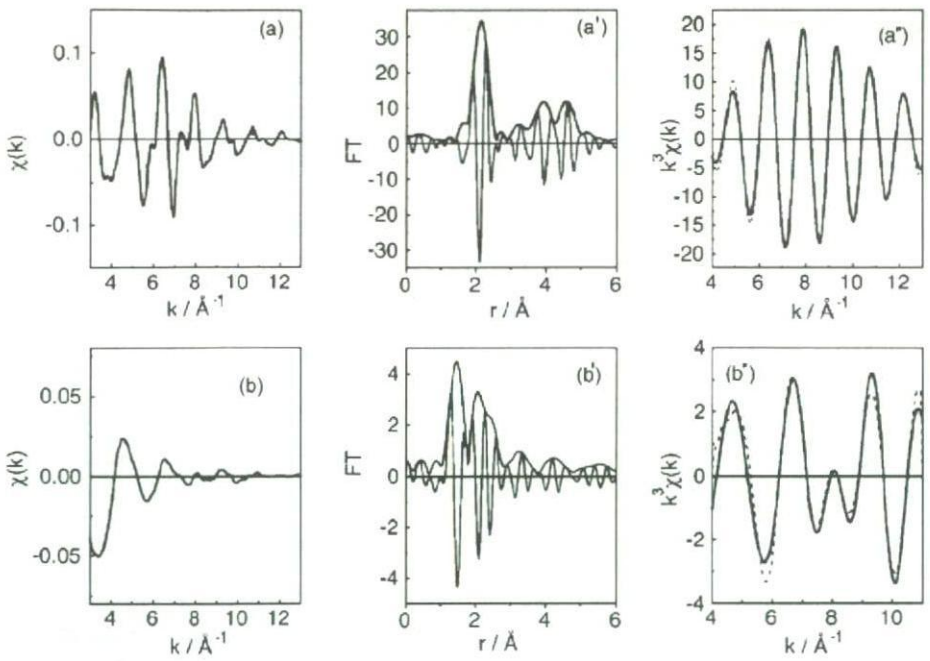

FIG. 2. (Color online) Ni *K*-edge EXAFS spectra (a,b), their Fourier transforms (a′,b′) and curve fitting results (a″,b″) before (a,a′,a″) and after the purification (b,b′,b″). In (a″) and (b″) the solid lines show the Fourier filtered EXAFS whereas the dashed lines show the fitted EXAFS.

Ni foil up to high k region; this result indicates the presence of Ni particles. Its Fourier transform has several peaks corresponding to those for Ni foil: Shape and pattern in 0–6 Å range are similar to those of the foil. The Ni particle size is estimated to be longer than 50 Å according to the Greegor's relationship between the size and the coordination numbers.[38] The result is consistent with the XRD and SEM data.[12] Table II shows the curve fitting results for the first shell of Ni in the CNF before purification. The coordination number is 10.8 after the reduction factor correction, which is slightly reduced from 12. This result may be caused by the intrinsic disorder in the Ni particles or the effect of impurity which is hardly observed in the EXAFS Fourier transform. As shown later, we still observe some deviation in the XANES spectrum before the purification from that of Ni foil, which indicate the presence of Ni-O bonding. We carry out two-shell fitting including Ni-O and Ni-Ni, and find better fitting results for the parameters listed in Table II, where R-factor 0.65% for the two-shell fitting is much smaller than 1.0% for the one shell fitting. The fitting EXAFS curve shows the excellent agreement with the observed one as shown in Fig. 2(a″).

After the purification, the EXAFS oscillation is different from that before the purification. The Fourier transform [Fig. 2(b′)] shows that the Ni-Ni peak at 2.1 Å decreases and a new peak appears around 1.4 Å which may correspond to the coordination of light atoms such as oxygen or carbon. As will be discussed in the XANES section, the peak corresponds to the Ni-C bond and we carry out the curve fitting analyses using carbon atoms: Results are shown in Table II. The coordination number and bond distance are 2.5 and 1.83 Å, respectively. For various Ni-C systems Ni-carbon bond distances are listed in Table III. The Ni-C in the CNF is shorter than Ni-C bonds found in $Ni(cp)_2$ (π bond) and other π bonding compounds. Thus we can rule out the possibility that Ni species form π bonds with carbon atoms in graphene aromatic rings. This means that the Ni-C bond is strongly bound to CNF through σ bond. Since bond lengths for the Ni-C "single bond" are longer than 1.90 Å, the "multiple bond" or some strong specific σ bond as formed in $Ni(CO)_4$ is presumably formed: Actually bond lengths for the Ni-C "double bonds" are in the range of 1.83–1.89 Å, and Ni-C distance is 1.82 Å in $Ni(CO)_4$.

The Ni impurities should occupy substitution site in the graphene sheet or edge site with strong Ni-C bonds. Such strong Ni-C bonds prevent the Ni atoms from being removed by the purification. In addition to the short Ni-C bonds, we find other peak around 2.3 Å, which corresponds to the

TABLE II. Curve fitting results for Ni species in CNF. r is the distance to the neighbor, σ is the Debye-Waller factor, ΔE is a shift in edge energy, R is R-factor defined by Eq. (1).

Sample	Bond	N[a]	r/Å	σ/10^{-2} Å	ΔE/eV	R/%	
Before	Ni-Ni	10.8±1.6	2.47±0.02	6.9±3.0	−7±7	1.0	One shell
	Ni-Ni	10.3±1.6	2.47±0.02	6.8±3.0	−7±7		Two shell
	Ni-O	0.8±0.4	2.01±0.03	7.3±3.5	−4±1	0.65	Two shell
After	Ni-C	2.4±0.8	1.83±0.05	6.0±3.0	3±5	5.6	
	Ni-Ni	0.8±0.3	2.48±0.05	5.5±2.0	7±7		

[a]Coordination numbers are corrected by the factor S. $S_{Ni\text{-}Ni}=0.9$ and $S_{Ni\text{-}C}=1.0$ are used.

TABLE III. Ni-C bond length for various Ni-C systems. r is the distance to the neighbor.

Bond type	r/Å	References
Single σ bond	1.90–2.01	56–59
σ bond with aromatic ring	1.90–1.93	60–63
"Double bond"	1.83–1.89	62 and 64
σ bond in metallocycle	1.81–1.91	59, 65, and 66
π bond with "double bond"	2.00–2.21	64, 67, and 68
π bond with "triple bond"	1.87–1.99	69–71
π bond with allyl	1.93–2.11	72 and 68
π with aromatic ring	1.95–2.16	72 and 73
Ni_3C	1.86	39
$Ni(CO)_4$	1.82	74
$Ni(C_5H_5)_2$	2.196	55

Ni-Ni bond distance in Ni foil. Curve fitting analysis shows that the bond distance is 2.48 Å and coordination number is 0.8. In our previous paper,[20] we thought the peak indicated the formation of the Ni dimer in the CNT, but the peak might rather be due to the Ni-Ni bonds in the residual Ni particles because the bond length is quite close to that in Ni foil. This point will be again discussed in the XANES section. Further EXAFS analyses about the location and the detailed structure can be limited because of the one-dimensional information inherent to EXAFS analysis and of the Ni low concentration. Thus we switch our attention to the XANES analysis.

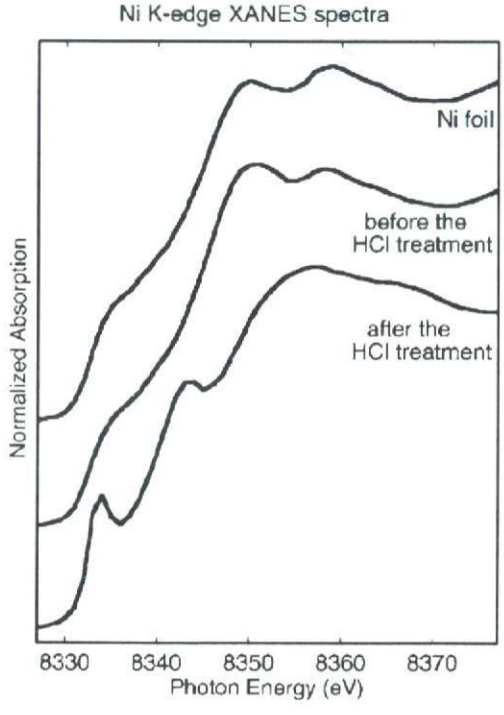

FIG. 3. The observed Ni K-edge XANES spectra of Ni species in the CNF before and after the purification together with that of Ni foil. The experimental data are normalized to the absorption intensity at 8400 eV.

B. XANES

Figure 3 shows the K-edge XANES spectra of Ni species in the CNFs before and after the purification together with that of Ni foil.[20] All the experimental data are normalized to the absorption intensity at 8400 eV, and the calculated atomic absorption cross sections are also normalized in the same way. The XANES spectrum after the purification shows prominent difference from that before the treatment which is quite similar to that for Ni foil. However, the peak at 8350 eV is a little larger than that at 8360 eV. Since $Ni(H_2O)_6(NO_3)_2$ has a peak around 8350 eV, we infer the presence of a small amount of $Ni(H_2O)_6^{2+}$ species. We analyze the observed data on the basis of a regression method using two reference spectra of Ni foil and of $Ni(H_2O)_6(NO_3)_2$ by adjusting the coefficients, c_1 and c_2,

$$\mu_{Ni_{CNF}} = c_1\mu_{foil} + c_2\mu_{Ni(H_2O)_6}, \tag{4}$$

$$c_1 + c_2 = 1, \tag{5}$$

where $\mu_{Ni_{CNF}}$, μ_{foil}, and $\mu_{Ni(H_2O)_6}$ are the Ni K-edge x-ray absorption intensities of Ni species in CNF, of Ni foil and of $Ni(H_2O)_6$. The best fit is obtained when we choose $c_1 = 0.88 \pm 0.05$ as shown in Fig. 4, which supports the presence

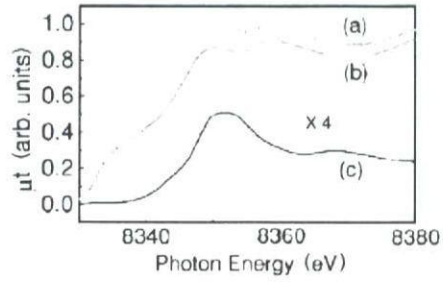

FIG. 4. (Color online) (a) the regression analysis of Ni species in the CNF before the purification. Solid line and circles are observed and best fitted data, respectively. Lines (b) and (c) are the spectra of Ni foil and $Ni(H_2O)_6(NO_3)_2$.

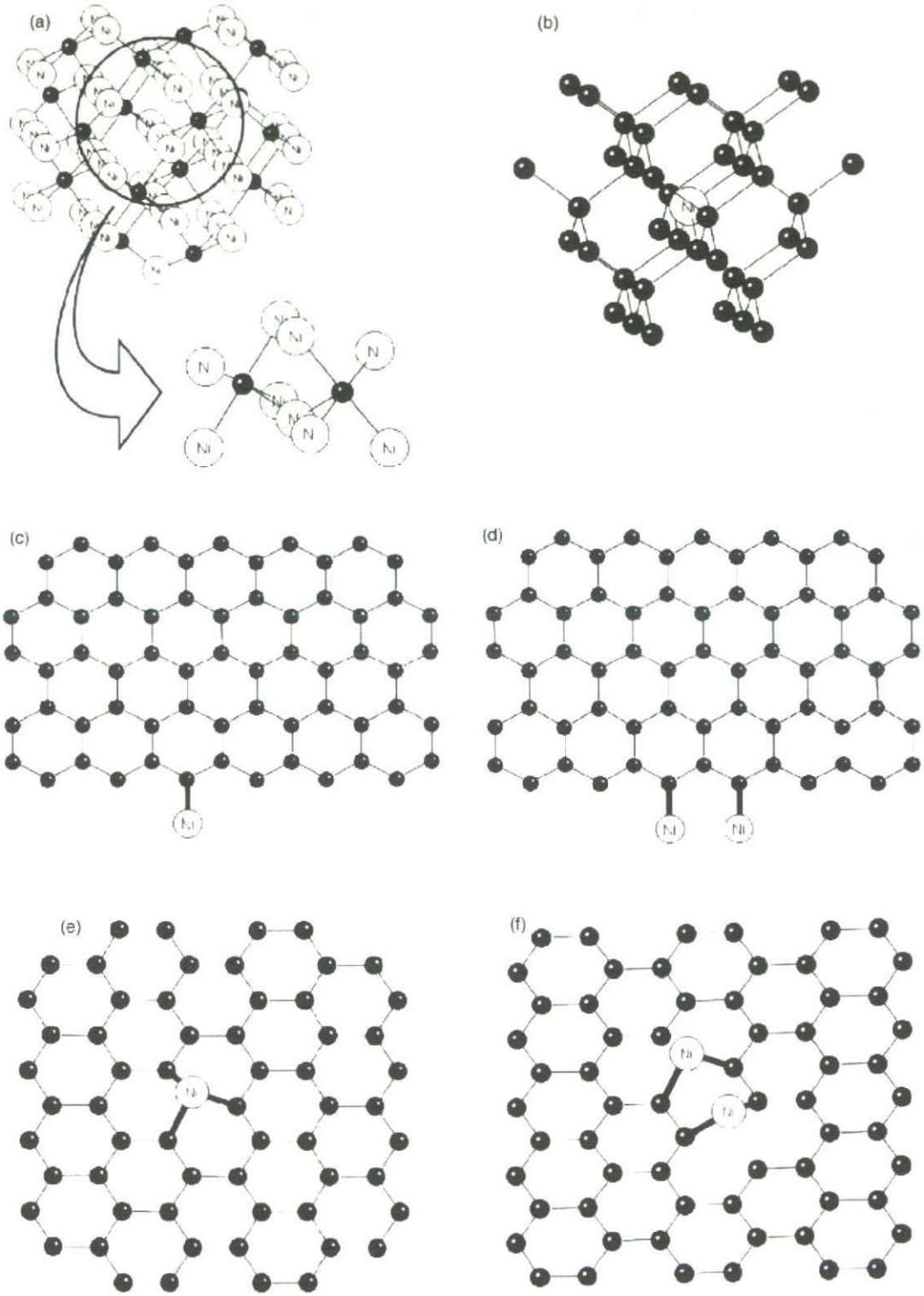

FIG. 5. Local structures of a carbide model (a) and a diamond model (b). In (a) each Ni atom is surrounded by two carbon atoms. In (b) each Ni atom is absorbed in the diamond and surrounded by four carbon atoms. In (c) and (d) edge models, and in (e) and (f) substitution models are shown.

of $Ni(H_2O)_6$ species. This conclusion does not contradict the EXAFS results obtained in the preceding section. The expected coordination number for Ni-Ni and Ni-O based on the c_1 and c_2 are 10.8 ± 0.6 and 0.72 ± 0.04, respectively, which are in good agreement with the estimated ones 10.3 ± 1.6 and 0.8 ± 0.4 by the EXAFS analyses shown in Table II.

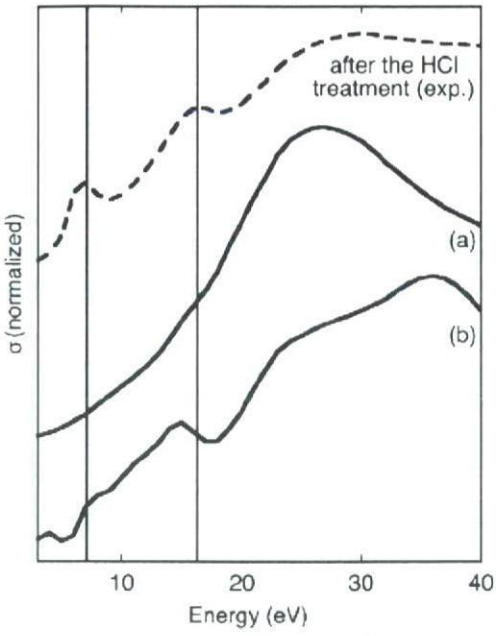

FIG. 6. Calculated XANES spectra for the carbide model (a) and a diamond model (b) shown in Fig. 5 compared with the experimental Ni K-edge XANES after the purification. The energy is measured from the onset of the K-edge absorption.

C. Multiple scattering analysis of XANES

The XANES spectrum after the purification is different from that before the purification. There are two characteristic peaks at the absorption edge regions. This characteristic structure should be the fingerprint for the calculated XANES spectra using multiple scattering theory for several model structures given in Figs. 5 and 9. We investigate the following possible models referring to other experimental findings and theoretical studies:

(1) a carbide model or a diamond model,
(2) an edge model,
(3) a substitution model,
(4) a Stone-Wales defect model.

In these calculations the Ni atoms are assumed to be neutral as supported by our DFT calculations.

1. A carbide model or a diamond model

Although the carbide, Ni_3C contains a quite large number of Ni-Ni pairs (coordination number 12) at 2.63 Å,[39] we consider the carbide model because carbide has often been observed during the catalytic reactions of Ni with CO and hydrocarbons. Figure 6(a) shows the calculated Ni K-edge XANES spectrum for the carbide model shown in Fig. 5(a) compared with the experimental spectrum after the purification. The agreement is quite poor as expected, since no specific peak is observed in the calculated spectrum.

Hayakawa *et al.* have reported micro XANES spectrum for the Ni impurities in the synthetic diamond.[40] They find similar two peaks in the near edge region of the Ni K-edge. The second peak appears at a little higher energy than the corresponding peak in the spectrum of the Ni species in the

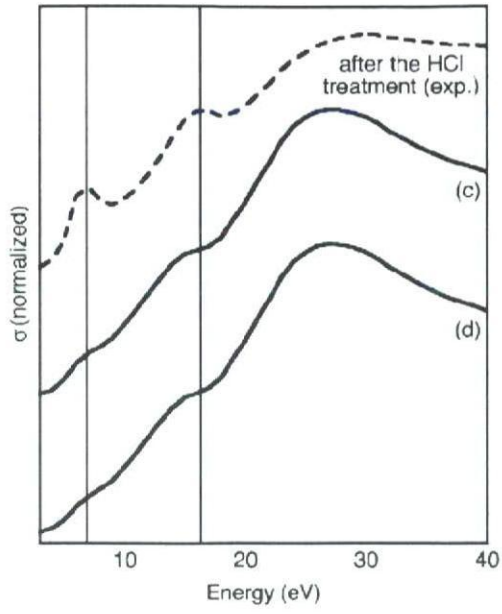

FIG. 7. The calculated XANES spectra for the edge models (c) and (d) shown in Fig. 5 compared with the experimental Ni K-edge XANES after the purification. The energy is measured from the onset of the K-edge absorption.

CNF. They propose a substitution model for the Ni site, i.e., a carbon is replaced by a Ni atom and the replaced Ni is surrounded by four carbon atoms in a tetrahedral symmetry. The model is shown in Fig. 5(b): Ni-C distance is assumed to be 1.8 Å with coordination number 4. The calculated XANES spectrum shown in Fig. 6(b) gives rise to two small peaks. However, the second peak position of the calculated

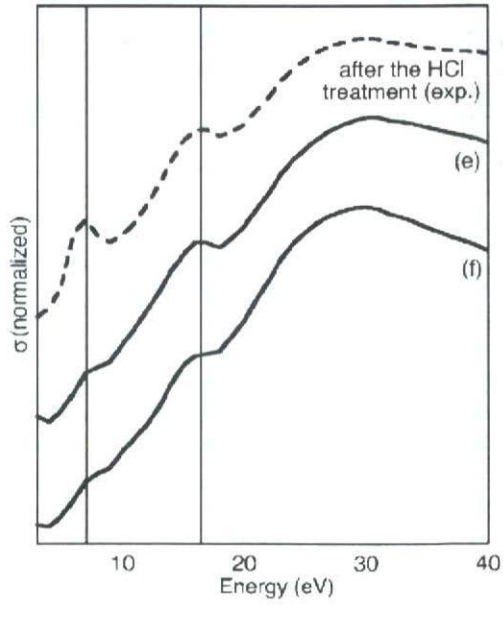

FIG. 8. Calculated Ni K-edge XANES spectra for the substitution models (e) a monomer model and (f) a dimer model compared with the observed spectrum after the purification. The energy is measured from the onset of the K-edge absorption.

XANES spectrum in Fig. 6(b) is different from that of Ni atoms in CNFs measured in this paper. Thus the diamond model is also rejected.

Ni in diamond has been investigated because Ni is a good catalyst for the synthesis of diamond and Ni is efficiently substituted into the diamond to modify the optical and physical properties. Hitherto EPR and theoretical studies have proposed several model structures for Ni impurities in diamond, which support the presence of substitutional Ni.[40,42] However, recent theoretical and ESR results show that the substitutional Ni are not so stable and they are accompanied with defects (one or two vacancies) or impurities (nitrogen).[41,43–46] Further analyses of Ni *K*-edge XANES in diamond should be necessary to confirm their local structures.

2. Edge models

Sharp has discussed the catalytic reaction mechanism for the synthesis of CNT based on the organometallic chemistry.[47] They propose metallocyclic species as an intermediate. At edges of graphene sheets carbon atoms have dangling bonds: Ni atoms can adsorb on the edge of a graphene sheet, forming covalent bonds with C atoms at the edges. We study two different edge models as shown in Figs. 5(c) and 5(d). In both models the Ni-C distance is assumed to be 1.8 Å with coordination number 1. In the latter model Ni dimer structure is assumed with the Ni-Ni distance 2.5 Å. The calculated spectra are shown in Fig. 7. Both models give nearly the same spectra which show quite small shoulders at 7 and 16 eV, and too rapid decrease above 30 eV. These models cannot sufficiently reproduce the observed features.

3. Substitution models

Ni can be on a substitution site in the graphene sheet. Meng *et al.* study the metal-graphene sheet interaction by Hartree-Fock calculations with approximate exchange potential.[13] Their results show strong attractive interaction and bonding with a graphene sheet due to the unfilled $3d$ shell for transition metals. A different theoretical work also supports the substitutional Ni atom in a CNT.[17]

We consider two substitution models—monomer and dimer. In the monomer model as shown in Fig. 5(e), Ni is bound to a graphene sheet through three C-Ni bonds with distance of 1.8 Å. In the dimer model shown in Fig. 5(f), a Ni dimer forms the two C-Ni bonds with the same distance (1.8 Å) and the coordination number 2. In the dimer the Ni-Ni distance is 2.5 Å with coordination number 1. These values are in accordance with the EXAFS results.[20] Figure 8 shows the calculated XANES for the monomer and dimer models shown in Figs. 5(e) and 5(f). We can well reproduce the two characteristic peaks at 7 and 16 eV by the monomer model, although the peak at 7 eV is a little weaker than the observed one. The peak at 7 eV is located just at the beginning of the edge rise and should have a contribution from the atomic bound state that cannot be fully taken into account by the present method. The 16 eV peak is in the continuum character and can successfully be calculated by the multiple scattering theory. The dimer model shows two features at 7 and 16 eV but the peak intensities are one-half of the Ni

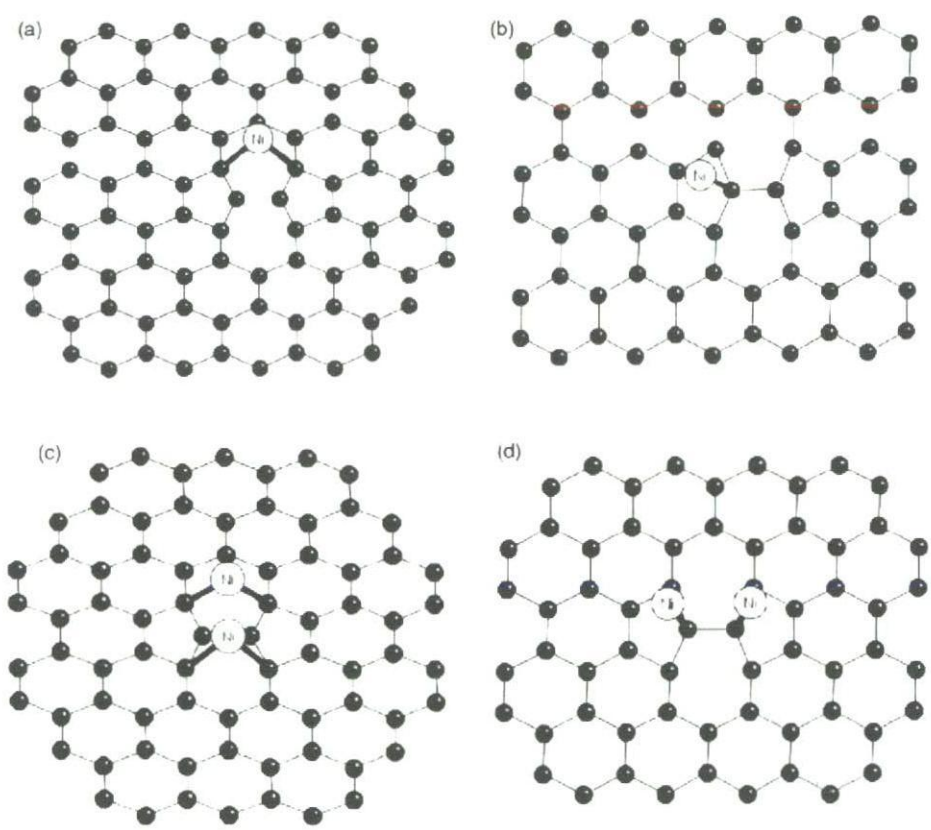

FIG. 9. Four defects models around the Stone-Wales defects. In the model (a) and (b) one Ni atom adsorbs on the 7 and 5 ring, respectively. In model (c) and (d) two Ni atoms adsorb on the 7 and 5 rings, respectively.

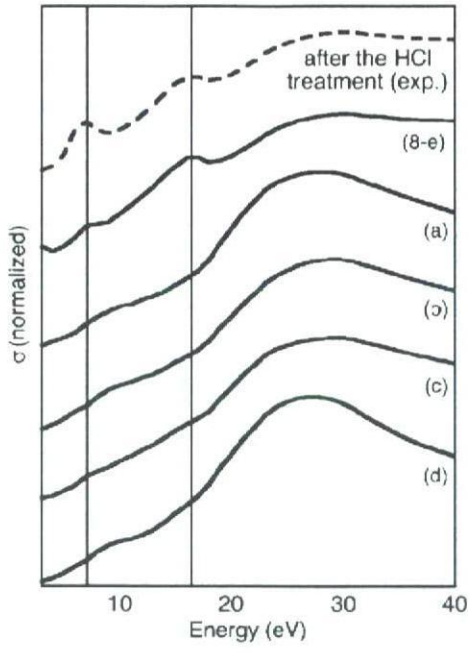

FIG. 10. Calculated Ni *K*-edge XANES spectra for the four models shown in Fig. 9 compared with the experimental spectrum after the purification. For the comparison the calculated spectrum for the model (e) in Fig. 8 is shown as (8-e). The energy is measured from the onset of the *K*-edge absorption.

monomer structure. The structure above 30 eV region is not well fitted to the observed one in the dimer structure. The CNF is composed of multilayer with interlayer distance 3.4 Å.[12,48] We add another sheet (two-sheet model), but we cannot find its remarkable effect on the calculated spectra since the bond length of the Ni-C in the next sheet is quite large.

We thus conclude that most of Ni impurities are in monomer structures in a graphene sheet; each of them substitutes a carbon atom.

4. Stone-Wales defect models

An important defect in the CNT is a Stone-Wales defect where a pair of 5–7 rings can be created by rotating a C-C bond in the hexagonal network by 90°.[49] Recent molecular orbital calculations show that the introduction of Stone-Wales defects would benefit the adsorption capacity of B, N, F, and Si among 10 foreign atoms (H, B, C, N, O, F, Si, P, Li, and Na).[50] This result suggests that the Stone-Wales defects can be the Ni adsorption sites. (See Figs. 9 and 10.) Figure 10 shows the XANES spectra based on the four models shown in Fig. 9. The adsorption models around the Stone-Wales defects (a)–(d) fail to explain the two specific peaks at 7 and 16 eV, and we can rule out the above models.

D. Comparison with literature

In our calculations, the substitution model shown in Fig. 5(e) gives good fit to the observed data. Takenaka *et al.* have also observed the two peaks discussed in this paper in the

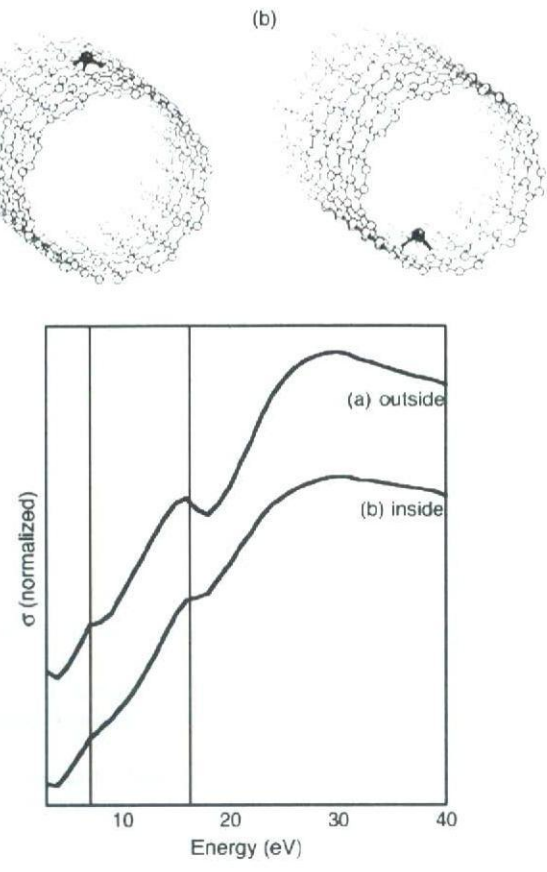

FIG. 11. Two tube models and the calculated XANES spectra. The tube type is armchair which is (10,10) tube with 14 Å in diameter. We assume that Ni atoms are present at the substitution sites whose local adsorption structures are nearly the same as those shown in Fig. 5(e). In model (a) the Ni is located outside of the tube, and in model (b) the Ni is located inside the tube. Calculated Ni *K*-edge XANES spectra are shown for the two tube models.

XANES spectra of the heavily deactivated Ni catalyst after the CH_4 decomposition reaction to carbon filament.[51] They compared the XANES and EXAFS of the "Ni carbide" with those of the known Ni_3C, and found that both spectra were completely different. This result clearly shows that the Ni carbide prepared from the methane decomposition is not the Ni_3C species. They were not able to determine the structure because the strong Ni-Ni peak in Fourier transformed EXAFS spectra for Ni particles were observed at the same time. Judging from the peak positions in the XANES spectra and Fourier transform peaks in the EXAFS, the deactivated Ni they observed should be the same one discussed in this work.

The proposed structure as shown in Fig. 5(e) has already been suggested by Banhart *et al.* in the onionlike graphitic networks.[18] They observe Ni atoms in graphitic carbon onions by TEM and observed a zigzag structure, which indicates the formation of a new C-Ni phase. Their first principle calculations show that the Ni-substituted graphite structure with C-Ni distance 1.8 Å is quite consistent with our XAFS results. Their Car-Pallinello simulation suggests the high stability of this substituted Ni atom in the graphene sheet. Andriotis *et al.* study Ni in a CNT framework using a tight